

# Pulsar winds: Transition to a Force-Free Regime

Z. Osmanov<sup>1</sup>, D. Shapakidze<sup>2</sup> and G. Machabeli<sup>3</sup>

*E. Kharadze Georgian National Astrophysical Observatory*

## ABSTRACT

The problem of reconstruction of the pulsar magnetospheres nearby the light cylinder surface is studied. It is shown that, on the basis of the Euler, continuity and induction equations, there is a possibility of parametrically excited rotational energy pumping process into the drift modes. As a result, the toroidal component of the magnetic field increases very rapidly. The increment is analyzed for plasma parameters of a typical pulsar magnetosphere. The feedback of the excited waves on the particles is considered to be insignificant. The dynamics of the reconstruction of the pulsar magnetosphere is studied analytically. It is traced from the generation of a toroidal component of the magnetic field up to transformation of the field lines into such a configuration, when plasma particles do not experience any forces: the motion of the particles switches to the so called 'force-free' regime. At this stage the generation of the toroidal component comes to the end, and the pulsar wind reaches its stationary state.

*Subject headings:* pulsars, instabilities, plasma

## 1. Introduction

One of the major problem for pulsar winds concerns the transition of the magnetized plasma flows through the so called 'light cylinder' surface - a hypothetical zone, where the linear velocity of rotation equals to the speed of light. According to the model of pulsar magnetosphere (Goldreich & Julian 1969), the relativistic plasma flow, emanating from the pulsar surface streams along very strong magnetic field lines. The typical values of the magnetic field are of the order of  $10^{12}$  G (Manchester & Taylor 1977). It is well known

---

<sup>1</sup>z.osmanov@astro-ge.org

<sup>2</sup>d.shapakidze@astro-ge.org

<sup>3</sup>g.machabeli@astro-ge.org

that such a huge magnetic field forces the particles to co-rotate with a pulsar. However the co-rotation of the magnetized plasma cannot be maintained nearby the light cylinder zone, stimulating the further exploration of this phenomenon.

The simplest idea explaining the transition of the plasma outflow through the light cylinder surface is to make the motion of the flow force-free at these distances [see e.g. Machabeli et al. (2000); Rogava et al. (2003)]. For this purpose, one needs to twist the field lines in a convenient manner. In other words, it is necessary to generate the toroidal component of the magnetic field. The pulsars maintain the dipolar magnetic field having a certain curvature of the field lines. The particles moving along the curved field lines are drifting perpendicularly to the curvature plane. The existence of the drift motion creates the necessary conditions for development the Curvature Drift Instability (CDI) (Kazbegi et. al 1989, 1991a,b; Shapakidze et. al 2003). The mechanism excites transverse drift modes providing the magnetic field with the toroidal component. The CDI becomes effective at the vicinity of the light cylinder surface, where the pulsar's dipolar field is sufficiently smaller in order to be compared with the toroidal component of the excited mode. Actually, the kinetic energy of the primary beam particles, having the density of Goldreich-Julian, can supply the generation of the drift waves. However, the kinetic energy density,  $W_b$ , of the primary beam is not sufficient to change significantly the configuration of the dipolar magnetic field,  $B_0$ , since  $W_b \ll B_0^2/(4\pi)$ . Therefore, the process of generation of the toroidal component,  $B_r$  (of the order of  $B_0$ ), requires an additional energy supply, which can be maintained by the pulsar rotational energy. We have already shown that the rotational energy pumping into the drift modes can be implemented by the "parametric" instability (Osmanov et al. 2008). This mechanism is called parametric, because the effect is provoked by the relativistic centrifugal force which, as a parameter, changes in time and induces the instability. The aim of the present paper is to study the saturation process of this instability. It will be shown below, that the saturation leads to the transition of the plasma outflow into the force-free regime nearby the light cylinder zone.

The problem analysis handles well if one considers the mechanical analog of the motion of plasma flow along the pulsar magnetic field lines and studies the dynamics of a single particle motion sliding inside the rotating channels. In the present paper we apply the method developed by Rogava et al. (2003) and study the plasma process which leads the configuration of the magnetic field lines to the Archimedes' spiral: it appears that in order to suppress the reaction force, the field lines, rather being straight, should deviate back and lag behind the rotation; consequently, in due course of time the curvature will increase, inevitably leading to the decrement of the reaction force; this process will last until the magnetic field lines get the shape of the Archimedes' spiral, that vanishes the reaction force saturating the instability.

The organization of the paper is the following: in Section 2 we study the conversion of kinematics of relativistic particle, sliding along the arms of rotating Archimedes' spiral, to the force-free regime. In Section 3 we examine the plasma mechanism of twisting of magnetic field lines due to the parametrically excited CDI in the vicinity of the light cylinder surface. The numerical estimations are provided in Section 4 and the results - summarized in Section 5.

## 2. Force-free Kinematics

Let us prescribe the configuration of magnetic field lines with the Archimedes' spiral:

$$\Phi = aR, \quad (1)$$

where  $\Phi$  and  $R$  are the polar coordinates and  $a = \text{const}$  (see Figure 1). Rogava et al. (2003) showed that the dynamics of the particle motion asymptotically tends to the force-free regime if the particle slides along the rotating channel having a shape of the Archimedes' spiral. However, in the Laboratory Frame (LF), the particle follows the straight linear paths with constant velocities. An observer from the LF will detect the following effective angular velocity:

$$\Omega_{ef} = \Omega + \frac{d\Phi}{dt} = \Omega + av, \quad (2)$$

where  $v$  is the radial velocity of a particle motion; and  $\Omega$  - the angular velocity of rotation. If the particle moves without acceleration in the LF, the corresponding effective angular velocity must be equal to zero. In this case Eq. (2) yields:

$$v = v_c \equiv -\frac{\Omega}{a}, \quad (3)$$

which means that, for each Archimedes' spiral with  $|a| > \Omega/c$  and  $a < 0$ , there exists a certain value of velocity,  $v_c$  (hereafter we call it "characteristic velocity"), when the LF trajectory of the particle is a straight line. The relativistic momentum of the particle writes as follows:

$$P_R = \gamma m v, \quad (4)$$

$$P_\Phi = \gamma m R \Omega_{ef}, \quad (5)$$

where  $m$  and  $\gamma$  are the rest mass and the Lorentz factor of the particle respectively.

The expansion of the equation of motion,  $d\mathbf{P}/dt = \mathbf{F}$  ( $\mathbf{F}$  is the reaction force), in terms of the radial component:

$$F_R = -\frac{aR}{\sqrt{1+a^2R^2}}|\mathbf{F}|, \quad (6)$$

and the angular component:

$$F_\Phi = \frac{1}{\sqrt{1+a^2R^2}}|\mathbf{F}|, \quad (7)$$

of the reaction force, yields the following equation (Rogava et al. 2003):

$$\frac{d^2R}{dt^2} = \frac{\Omega - \gamma^2 v(a + \Omega v/c^2)}{\gamma^2 \kappa^2} \Omega_{ef} R, \quad (8)$$

where

$$\kappa \equiv \left(1 - \frac{\Omega^2 R^2}{c^2} + a^2 R^2\right)^{1/2}.$$

Note that  $(d^2R/dt^2) \equiv 0$ , when  $v = -\Omega/a$ .

Since we are interested in relativistic flows, let us consider  $v_c = c$  setting  $a = -\Omega/c$ . In Figure 2 we show the dependence of  $\beta_R \equiv v/c$  versus  $R/R_c$  ( $R_c$  is the light cylinder radius) for the different initial values of  $\beta_{R0}$ . As it is clear from these plots, even though the initial velocity of particles is weakly relativistic (e.g.  $\beta_{R0} = 0.01$ ), it will asymptotically tend to the characteristic velocity,  $v_c$ . As a result, the particle trajectory in the LF must become linear.

Indeed, in Figure 3 we show the particle trajectory in the Rotational Frame (RF) of reference (see Fig.3a) as well as in the LF (see Fig.3b) for  $\beta_{R0} = 0.01$  and for the same spiral configuration with  $a = -\Omega/c$ . Observing the particle trajectory from the LF, one can notice that the path asymptotically becomes linear, indicating the conversion of the particle motion to the force-free regime. Therefore, we conclude that the magnetic field having a shape of the Archimedes' spiral may guarantee the transition of the plasma flow through the light cylinder surface.

In the next section we consider the possible plasma mechanism for twisting the quasi-straight magnetic field lines in the magnetosphere.

### 3. Parametrically Excited Curvature Drift Instability

It is well known, that the presence of an external variable parameter usually generates the plasma instability. For example, the mechanism of energy pumping process from the external alternating electric field into the electron-ion plasma is quite well investigated (Silin

1973; Galeev & Sagdeev 1973; Max 1994). Although the physics of the parametric instability in the electron-ion plasma differs from that of the electron-positron ( $e^+e^-$ ) plasma, the techniques of calculation can be the same. In the case of  $e^+e^-$  plasma the variable external parameter is the altering centrifugal acceleration (Machabeli et al. 2005).

We start our consideration initially supposing that the magnetic field lines are almost straight with very small non zero curvature (see Fig. 4a). The plasma stream is supposed to be moving along the co-rotating field lines provided by the strong magnetic field ( $\sim 10^{12}$  G for typical pulsars). We assume that the plasma flow is composed of two components: the plasma component ( $pl$ ) and, the so called, beam component ( $b$ ). The dynamics of plasma particles moving along the straight rotating magnetic field lines is described by the Euler equation (Machabeli et al. 2005)

$$\frac{\partial \mathbf{p}_\alpha}{\partial t} + (\mathbf{v}_\alpha \nabla) \mathbf{p}_\alpha = -\gamma_\alpha \xi \nabla \xi + \frac{e}{m} (\mathbf{E} + \mathbf{v}_\alpha \times \mathbf{B}), \quad (9)$$

where

$$\xi \equiv \sqrt{1 - \Omega^2 R^2 / c^2};$$

$R$  is the coordinate along the straight field lines;  $\alpha = \{pl, b\}$  denotes the sort of particles;  $\mathbf{p}_\alpha$ ,  $\mathbf{v}_\alpha$ , and  $e$  are the momentum, the velocity and the charge of electrons, respectively;  $\mathbf{E}$  is the electric field and  $\mathbf{B}$  is the magnetic field. On the right hand side of Eq. (9) there are two major terms, from which the first represents the centrifugal force and the second - the Lorentz force. The full set of equations for  $n$ ,  $\mathbf{v}$ ,  $\mathbf{p}$ ,  $\mathbf{E}$  and  $\mathbf{B}$  should be completed by the continuity equation:

$$\frac{\partial n_\alpha}{\partial t} + \nabla(n_\alpha \mathbf{v}_\alpha) = 0, \quad (10)$$

and the induction equation:

$$\nabla \times \mathbf{B} = \frac{1}{c} \frac{\partial \mathbf{E}}{\partial t} + \frac{4\pi}{c} \sum_{\alpha=pl,b} \mathbf{J}_\alpha, \quad (11)$$

where  $n_\alpha$  and  $\mathbf{J}_\alpha$  are the density and the current, respectively.

Rewriting the Euler equation for the leading state and taking into account the frozen-in condition:  $\mathbf{E}_0 + \mathbf{v}_{0\alpha} \times \mathbf{B}_0 = \mathbf{0}$ , Eq. (9) reduces to Eq. (8). For the ultra relativistic particles, pulling out the axis of rotation, the solution of Eq. (8) writes as follows (Machabeli & Rogava 1994):

$$v_\theta^0 \equiv v_\parallel = c \cos(\Omega t), \quad (12)$$

where  $v_\parallel$  denotes the velocity component along the magnetic field lines.

In due course of time, the centrifugal force causes the separation of charges in plasma consisting of several species. This process becomes so important that the corresponding electromagnetic field affects the dynamics of charged particles. Therefore, the produced electric field should also be considered in the Euler equation (9) as the next term of approximation (Osmanov et al. 2008).

To make mathematics tractable, we will linearize the set of Eqs. (9-11), supposing that, in the zeroth approximation, the flow has the longitudinal velocity satisfying Eq. (12), and it also drifts along the  $x$ -axis due to the curvature of magnetic field lines (see Fig. 4):

$$u_\alpha = \frac{\gamma_{\alpha 0} v_\parallel^2}{\omega_B R_B}, \quad (13)$$

where  $u_\alpha$  is the drift velocity,  $\omega_B = eB_0/mc$ ;  $R_B$  is the curvature radius of magnetic field lines; and  $B_0$  - the magnetic induction in the leading state. In our case, the curvature drift contributes in  $\mathbf{J}$  [see Eq. (11)] as a source of an additional current. Note that the numerical simulations implementing the electric drift current (Blandford 2002) was considered by Spitkovsky & Arons (2002) and Spitkovsky (2004).

Let us represent all physical quantities as sum of the zeroth and the first order terms:

$$\Psi \approx \Psi^0 + \Psi^1, \quad (14)$$

where

$$\Psi \equiv \{n, \mathbf{v}, \mathbf{p}, \mathbf{E}, \mathbf{B}\}.$$

Then expressing the perturbed quantities as follows:

$$\Psi^1(t, \mathbf{r}) \propto \Psi^1(t) \exp [i(\mathbf{k}\mathbf{r})], \quad (15)$$

examining only the  $x$  components of Eqs. (9,11) and bearing in mind that  $v_\parallel^1 \approx cE_x^1/B_0$  and  $k_\theta \ll k_x$ , one can easily reduce the set of Eqs. (9-11) to the following form:

$$\frac{\partial p_{\alpha x}^1}{\partial t} - i(k_x u_\alpha + k_\theta v_\parallel) p_{\alpha x}^1 = \frac{e}{c} v_\parallel B_r^1, \quad (16)$$

$$\frac{\partial n_\alpha^1}{\partial t} - i(k_x u_\alpha + k_\theta v_\parallel) n_\alpha^1 = ik_x n_\alpha^0 v_{\alpha x}^1, \quad (17)$$

$$-ik_\theta c B_r^1 = 4\pi e \sum_{\alpha=pl,b} (n_\alpha^0 v_{\alpha x}^1 + n_\alpha^1 v_\parallel). \quad (18)$$

Introducing a special ansatz for  $v_{\alpha x}^1$  and  $n_\alpha^1$ :

$$v_{\alpha_x}^1 \equiv V_{\alpha_x} e^{i\mathbf{k}\mathbf{A}_\alpha(t)}, \quad (19)$$

$$n_\alpha^1 \equiv N_\alpha e^{i\mathbf{k}\mathbf{A}_\alpha(t)}, \quad (20)$$

where

$$A_{\alpha_x}(t) = \frac{u_\alpha t}{2} + \frac{u_\alpha}{4\Omega} \sin(2\Omega t), \quad (21)$$

$$A_{\alpha_\theta}(t) = \frac{c}{\Omega} \sin(\Omega t) \quad (22)$$

and substituting Eqs. (19,20) into Eqs. (16,17), one gets the following expressions:

$$v_{\alpha_x}^1 = \frac{e}{m\gamma_{\alpha_0}} e^{i\mathbf{k}\mathbf{A}_\alpha(t)} \int^t e^{-i\mathbf{k}\mathbf{A}_\alpha(t')} v_{\parallel}(t') B_r(t') dt', \quad (23)$$

$$n_\alpha^1 = \frac{ien_\alpha^0 k_x}{m\gamma_{\alpha_0}} e^{i\mathbf{k}\mathbf{A}_\alpha(t)} \int^t dt' \int^{t''} e^{-i\mathbf{k}\mathbf{A}_\alpha(t'')} v_{\parallel}(t'') B_r(t'') dt''. \quad (24)$$

Combining Eqs. (23,24) with Eq. (18), it is straightforward to reduce it into the following form:

$$\begin{aligned} -ik_\theta c B_r^1(t) &= \sum_{\alpha=pl,b} \frac{\omega_\alpha^2}{\gamma_{\alpha_0}} e^{i\mathbf{k}\mathbf{A}_\alpha(t)} \int^t e^{-i\mathbf{k}\mathbf{A}_\alpha(t')} v_{\parallel}(t') B_r(t') dt' + \\ i \sum_{\alpha=pl,b} \frac{\omega_\alpha^2}{\gamma_{\alpha_0}} k_x u_\alpha e^{i\mathbf{k}\mathbf{A}_\alpha(t)} &\int^t dt' \int^{t''} e^{-i\mathbf{k}\mathbf{A}_\alpha(t'')} v_{\parallel}(t'') B_r(t'') dt''. \end{aligned} \quad (25)$$

Here  $\omega_\alpha = e\sqrt{4\pi n_\alpha^0/m}$  is the plasma frequency. In order to simplify Eq. (25), one may use the following identity:

$$e^{\pm i x \sin \Omega t} = \sum_s J_s(x) e^{\pm i s \Omega t}. \quad (26)$$

Then Eq. (25) reduces to:

$$\begin{aligned} B_r(\omega) &= - \sum_{\alpha=pl,b} \frac{\omega_\alpha^2}{2\gamma_{\alpha_0} k_\theta c} \sum_{\sigma=\pm 1} \sum_{s,n,l,p} \frac{J_s(g_\alpha) J_n(h) J_l(g_\alpha) J_p(h)}{\omega + \frac{k_x u_\alpha}{2} + \Omega(2s+n)} \times \\ &\times B_r(\omega + \Omega(2[s-l] + n - p + \sigma)) \left[ 1 - \frac{k_x u_\alpha}{\omega + \frac{k_x u_\alpha}{2} + \Omega(2s+n)} \right] + \end{aligned}$$

$$\begin{aligned}
& + \sum_{\alpha=pl,b} \frac{\omega_\alpha^2 k_x u_\alpha}{4\gamma_{\alpha 0} k_\theta c} \sum_{\sigma, \mu=\pm 1} \sum_{s,n,l,p} \frac{J_s(g_\alpha) J_n(h) J_l(g_\alpha) J_p(h)}{\left(\omega + \frac{k_x u_\alpha}{2} + \Omega(2[s + \mu] + n)\right)^2} \times \\
& \times B_r(\omega + \Omega(2[s - l + \mu] + n - p + \sigma)),
\end{aligned} \tag{27}$$

where

$$g_\alpha = \frac{k_x u_\alpha}{4\Omega}, \quad h = \frac{k_\theta c}{\Omega}.$$

In order to solve Eq. (27) one has to examine similar equations, rewriting Eq. (27) for  $B_r(\omega \pm \Omega)$ ,  $B_r(\omega \pm 2\Omega)$ , etc.. This means that one has to solve the system with the infinite number of equations, which makes the problem impossible to handle. Therefore, the only way is to consider physics close to the resonance condition, which provides the cutoff of the infinite row in Eq.(27) making the problem solvable (Silin & Tikhonchuk 1970).

Let us consider the resonance condition, which corresponds to the curvature drift modes. As it is clear from Eq. (27), the proper frequency for the CDI equals:

$$\omega_0 \approx -\frac{k_x u_\alpha}{2}. \tag{28}$$

Therefore, physically meaningful solutions relate the case, when  $k_x u_\alpha/2 < 0$ . The present condition implies that  $2s + n = 0$  and  $2[s + \mu] + n = 0$ . On the other hand, one can easily check that, for the typical quantities  $\gamma_b \sim 10^6$ ,  $\lambda \sim 6 \times 10^{10} \div 3 \times 10^{11} cm$  (where  $\lambda \approx \lambda_x = 1/k_x$  is the wave length) of *1-second pulsars*,  $|k_x u_\alpha/2| \sim (0.02 \div 0.1)s^{-1}$  (here, it is supposed that  $k_x < 0$  and  $u_b > 0$ , otherwise the resonance frequency would be negative). Note, that this value is much less than  $\Omega(2s + n)$  and  $\Omega(2[s + \mu] + n)$  for non vanishing  $s$  and  $n$ . Consequently, the corresponding terms become rapidly oscillative and their contribution tends to zero. Therefore, preserving only the leading terms of Eq. (27) (also taking into account that the beam components exceed the corresponding plasma terms by many orders of magnitude), one gets the dispersion relation for the CDI (Osmanov et al. 2008):

$$\left(\omega + \frac{k_x u_b}{2}\right)^2 \approx \sum_{\sigma=\pm 1} \sum_{\mu=0,\pm 1} \sum_{s,l} \Xi_\mu J_s(g_b) J_{-2(s+\mu)}(h) J_l(g_b) J_{-2l+\sigma}(h), \tag{29}$$

$$\Xi_0 = 2\Xi_{\pm 1} = \frac{\omega_b^2 k_x u_b}{2\gamma_{b0} k_\theta c}. \tag{30}$$

In order to find the CDI growth rate,  $\Gamma$ , let us write  $\omega \equiv \omega_0 + i\Gamma$  and substitute to Eq. (29). As a result the imaginary part of Eq (29) writes as follows:

$$\Gamma \approx \left[ \sum_{\sigma=\pm 1} \sum_{\mu=0,\pm 1} \sum_{s,l} \Xi_\mu J_s(g_b) J_{-2(s+\mu)}(h) J_l(g_b) J_{-2l+\sigma}(h) \right]^{\frac{1}{2}}. \tag{31}$$



Now we can qualitatively analyze how does the shape of magnetic field lines change with time. After perturbing the magnetic field in the transverse direction, the toroidal component will grow and the shape of the field lines will gradually transform to that of the Archimede's spiral. From the simple considerations we can estimate the corresponding time scale of this transformation. Indeed, referring to Figure 4b,  $\tan \chi = B_r/B_\theta$ . On the other hand, the equation of Archimedes' spiral yields  $\tan \chi = aR$  resulting in  $B_r/B_\theta = aR$ . The toroidal component of magnetic field behaves with time as

$$B_r \approx B_r^0 e^{\Gamma t}$$

where  $B_r^0$  denotes the initial perturbed value of the toroidal component. Consequently, for the ultra-relativistic particles ( $a = -\Omega/c$ ) moving LC nearby zone ( $R \approx R_c$ ), the time scale of the process can be estimated as follows:

$$T \approx -\frac{1}{\Gamma(\lambda_x)} \ln \left( \frac{B_r^0}{B_\theta} \right). \quad (32)$$

#### 4. Discussion

Let us consider Eq. (32) and plot the time scale of the instability versus the wave length,  $\lambda_x$ , for several values of initial toroidal perturbations  $B_r^0$ . In Figure 5 we display the behavior of  $T(\lambda_x)$  for several values of the initial perturbation:  $B_r^0/B_\theta \equiv \delta \in \{10^{-1}; 10^{-3}; 10^{-5}; 10^{-7}\}$ . Two major applications are examined: *1-second* pulsar (a) and the Crab pulsar (b). It comes out from Eq. (32) that the time scale is a continuously decreasing function of the initial perturbation,  $B_r^0$ : as smaller is  $\delta$  parameter as smaller is the initial perturbation and, consequently, the magnetic field lines need more time to achieve the required structure.

The reconstruction of the magnetic field requires a certain amount of energy, therefore it is essential to estimate pulsar's slowdown luminosity ( $L_p$ ) and compare it to the, so called, "magnetic luminosity" ( $L_m \equiv \Delta E_m/T$ , where  $\Delta E_m$  is the variation of the magnetic field energy due to the instability). For  $L_p$  one has:

$$L_p = I\Omega\dot{\Omega} = I \frac{4\pi^2 \dot{P}}{P^2 P}, \quad (33)$$

where  $I \sim MR_p^2$  is the moment of inertia of the pulsar;  $M \sim M_\odot \approx 2 \times 10^{33} g$  and  $R_p \sim 10^6 cm$  pulsar's mass and radius, respectively. For typical pulsars,  $\dot{P}/P \sim 10^{-15} s^{-1}$ , the slowdown luminosity estimates as follows:

$$L_p \approx 7.9 \times 10^{31} erg/s. \quad (34)$$

The "magnetic luminosity",  $L_m$ , can be estimated straightforwardly:

$$L_m = \frac{B_r^2}{4\pi T} \Delta V, \quad (35)$$

where  $\Delta V \sim R_c^2 \Delta r = R_c^3 \varepsilon$  ( $\varepsilon \equiv \Delta r/R_c \ll 1$ ) is the volume, where the process of twisting takes place. Since we are studying the instability in the nearby zone of the LC, the magnetic field components must be given properly:  $B_r^0 \sim \delta \cdot B_\theta = \delta \cdot B_p (R_p/R_c)^3$ , where  $B_p \sim 10^{12} G$  is the magnetic field near the pulsar's surface. Substituting all quantities into Eq. (35) corresponding to the energy gain for  $\lambda_x \sim 2.5 \times 10^{11} cm$ ,  $T \approx 10^3 s$ , (see Fig. 5a), and bearing in mind Eqs. (3,32), one can show that for  $\varepsilon \sim 0.1$  and  $\delta \sim 0.1$  the value of the "magnetic luminosity" approximately equals:

$$L_m \approx 7.3 \times 10^{25} erg/s. \quad (36)$$

A direct comparison of Eqs. (34,36) exhibits:  $L_m \ll L_p$ , meaning that approximately only 0.0001% of the total energy budget goes to the reconstruction of the magnetic field lines.

In Figure 5b we show the behavior  $T(\lambda_x)$  for the Crab pulsar in the different cases of initial magnetic perturbations. The dependence does not change qualitatively but the twisting process changes quantitatively as the corresponding time scale is now of the order of  $\sim 10 \div 10^2 s$ . The "magnetic luminosity" of the Crab pulsar for  $\delta = 0.1$ ,  $\lambda_x = 7 \times 10^6 cm$ ,  $T \approx 4 s$  (see Fig. 5b), and  $\varepsilon = 0.1$  approximately equals [see Eq. (35)]:

$$L_m^{Crab} \approx 4.7 \times 10^{32} erg/s. \quad (37)$$

On the other hand a direct calculations of the Crab pulsar ( $P \approx 0.033 s$ ) luminosity, estimated by Eq. (33), yields:

$$L_p^{Crab} \approx 9.3 \times 10^{38} erg/s. \quad (38)$$

Therefore, also in the case of the Crab pulsar, the energy required for the reconstruction of the magnetosphere averages  $\sim 0.00005\%$  of the pulsar's energy and the twisting process becomes feasible in this case as well.

Generally speaking, in order to estimate how efficient is the instability, one has to compare its characteristic time scale to the pulsar's slowdown rate,  $P/\dot{P}$ . As observations show, this ratio ranges from  $10^{11} s$  (PSR 0531 - Crab pulsar) to  $10^{18} s$  (PSR 1952+29). But the greatest values of the twisting time scales, shown in Figure 5a,b, vary between  $10^4 s$  and  $10^2 s$ , which are less by many orders of magnitude than  $P/\dot{P}$ . The sweepback mechanism described in this paper, therefore, appears to be extremely efficient for typical pulsar magnetospheres.

The Cherenkov Drift Instability may result the reconstruction of the magnetic field lines in such a way, that the dynamics of magnetosphere becomes force-free. In the force-free regime the plasma of the pulsar magnetosphere makes its way through the light cylinder surface unhindered, skipping actually the LC problem at all.

## 5. Summary

1. Examining the pulsar magnetospheric relativistic plasma, we have studied the role of the parametrically excited CDI in the process of sweepback of magnetic field lines and the saturation process of the instability.
2. The linear analysis of the Euler, continuity and induction equations yields the dispersion relation governing the CDI.
3. Considering the resonance frequencies of the sweepback process, an expression of the instability increment has been obtained.
4. On the basis of the expression of the instability growth rate, we have derived the formula of the transition time scale of quasi-linear configuration of field lines into the Archimedes' spiral. The particles' motion is force-free along such magnetic field lines.
5. The transition time scale has been studied versus the wave length for the typical *1-second* pulsars and the Crab pulsar. For the both cases it was shown that the corresponding time scale is less than pulsar's spin down rates by many orders of magnitude indicating high efficiency of the discussed process.

The research was supported by the Georgian National Science Foundation grant GNSF/ST06/4-096.

## REFERENCES

- Blandford R.D., 2002, *luml. conf.*, 381B
- Galeev & Sagdeev, 1973, *Nucl. Fusion*, 13, 603
- Goldreich, P. & Julian, W.H., 1969, *ApJ*, 157, 869
- Kazbegi A.Z., Machabeli G.Z. & Melikidze G.I., in *Joint Varenna-Abastumani International School & Workshop on Plasma Astrophysics*, volume ESA SP-285, edited by T.D. Guyenne, (European Space Agency, Paris, 1989), p. 277
- Kazbegi A.Z., Machabeli G.Z. & Melikidze G.I., 1991a, *MNRAS*, 253, 377
- Kazbegi A.Z., Machabeli G.Z. & Melikidze G.I., 1991b, *Aust. J. Phys.* 44, 573.

- Machabeli G.Z., Mchedlishvili G.Z., & Shapakidze D.E., 2000, *Ap&SS*, 271, 277
- Machabeli G., Osmanov Z. & Mahajan S., 2005, *Phys. Plasmas* 12, 062901
- Machabeli, G.Z. & Rogava, A. D., 1994, *Phys.Rev. A*, 50, 98
- Manchester R. N. & Taylor J. H., 1977, *Pulsars* (ed.: W. H. Freeman and Company: San Francisco)
- Max C., 1973, *Phys. Fluids*, 16, 1480
- Osmanov, Z., Dalakishvili, Z. & Machabeli, Z. 2008, *MNRAS*, 383, 1007
- Rogava, A. D., Dalakishvili, G. & Osmanov, Z.N., 2003, *Gen. Rel. and Grav.* 35, 1133
- Shapakide, D., Machabeli, G. Melikidze, G., & Khechinashvili, D., 2003, *Phys.Rev.E*, **67**, 026407
- Silin V.P. & Tikhonchuk V.T., 1970, *J. Appl. Mech. Tech. Phys.*, **11**, 922
- Silin V.P., 1973, 'Parametricheskoe Vozdeistvie izluchenija bol'shoj mosshnosti na plazmu', Nauka, Moskva
- Spitkovsky A., 2004, 'Young Neutron Stars and Their Environments, IAU Symposium no. 218, held as part of the IAU General Assembly, 14-17 July, 2003 in Sydney, Australia. Edited by Fernando Camilo and Bryan M. Gaensler. San Francisco, CA: Astronomical Society of the Pacific, 2004, p.357
- Spitkovsky A. & Arons J., 2002, *ASP Conf. Ser.*, **271**, 81S

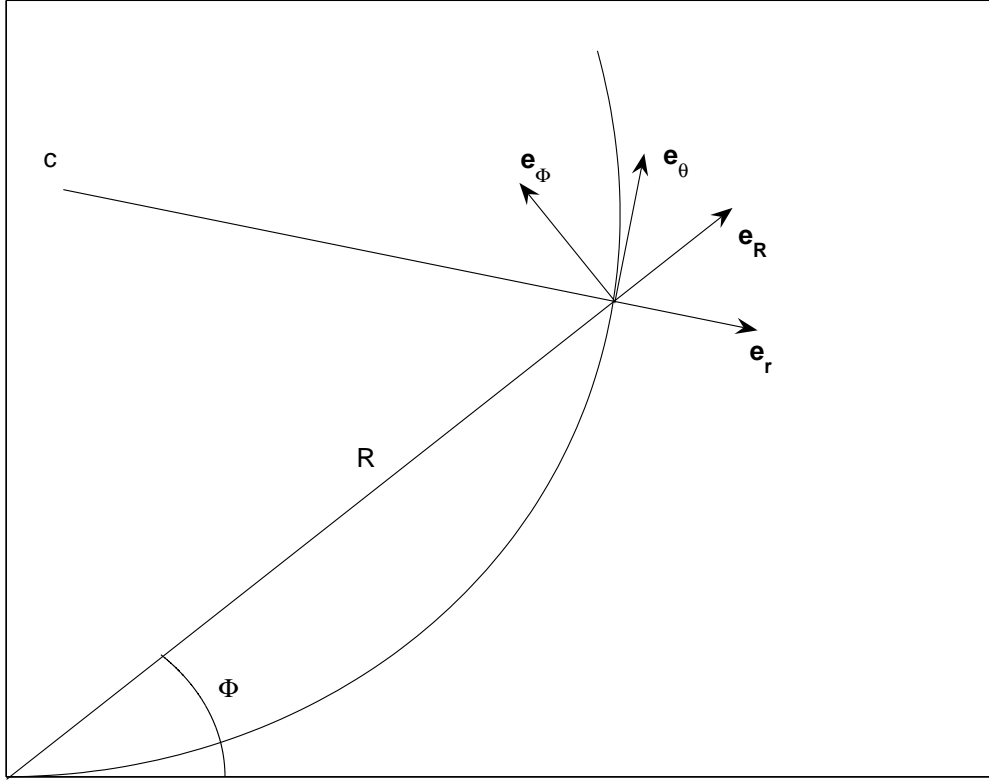


Fig. 1.— The arm of Archimedes spiral in polar coordinates  $(\Phi, R)$ . Two orthonormal bases are considered: i) polar components of unit vectors,  $(\mathbf{e}_\Phi, \mathbf{e}_R)$ ; ii) normal and tangential components of unit vectors,  $(\mathbf{e}_r, \mathbf{e}_\theta)$ , respectively.  $C$  is the center of the curvature.

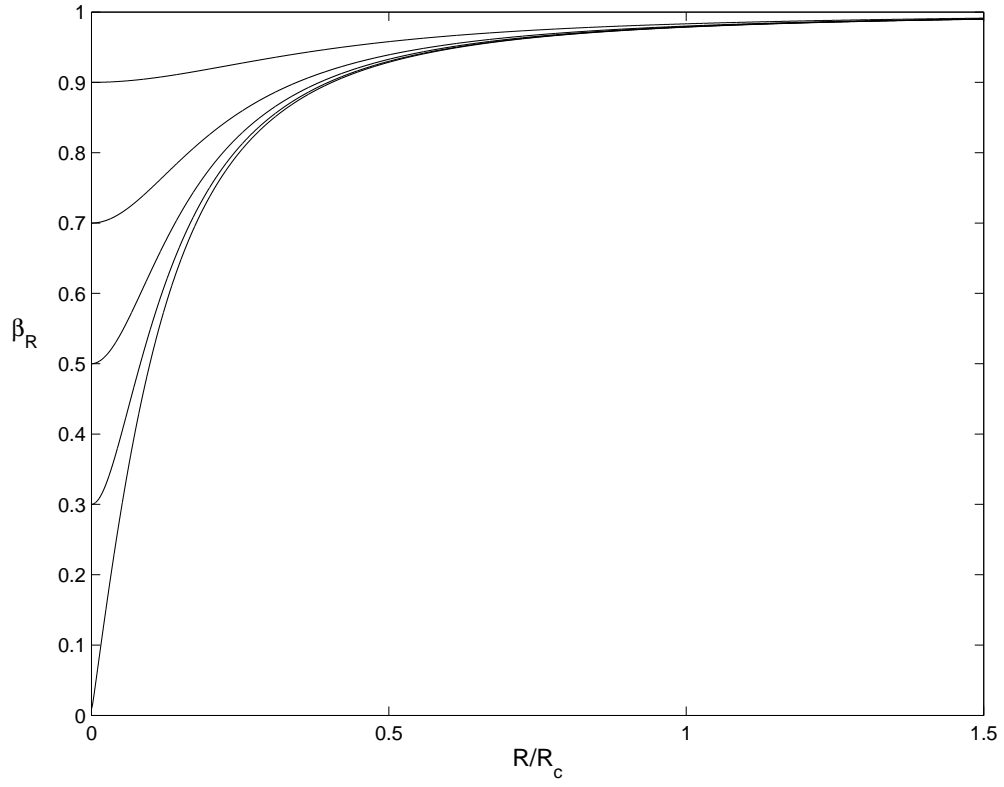


Fig. 2.— Behaviour of  $\beta_R$  versus  $R/R_c$ . The set of parameters is  $P = 1s$ ,  $\beta_{R0} = \{0.01; 0.3; 0.5; 0.7; 0.9\}$ .

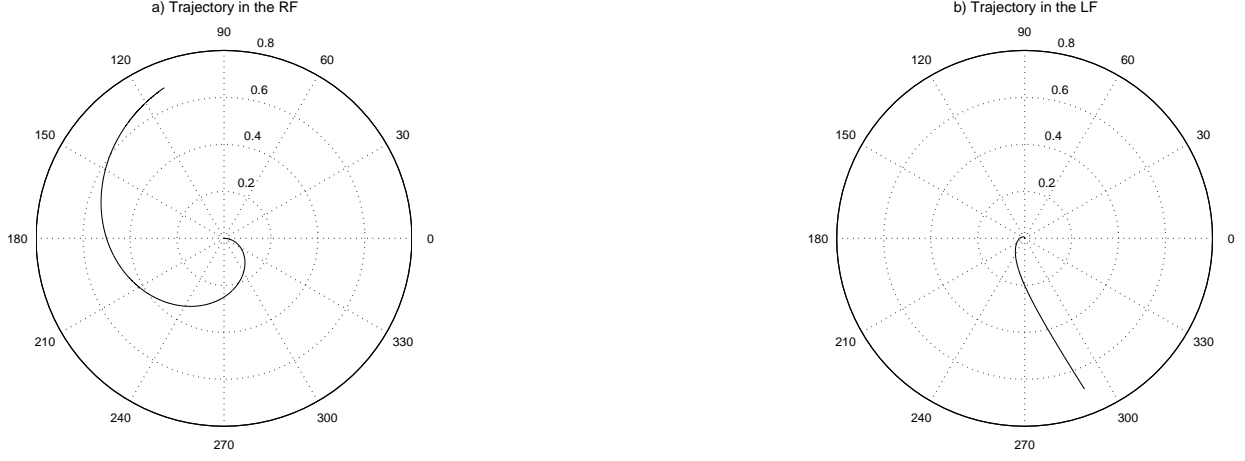


Fig. 3.— *a)* The trajectory of a particle in the Rotational Frame (RF) of reference; and *b)* the trajectory of a particle in the Laboratory Frame (LF) of reference. The set of parameters is  $P = 1s$  and  $\beta_{R0}^1 = 0.01$ . The radial distances are taken in terms of the light cylinder radius,  $R/R_c$ . The trajectory of the particle in RF follows the Archimedes' spiral (*a*), while the trajectory in the LF asymptotically tends to a straight line configuration (*b*).

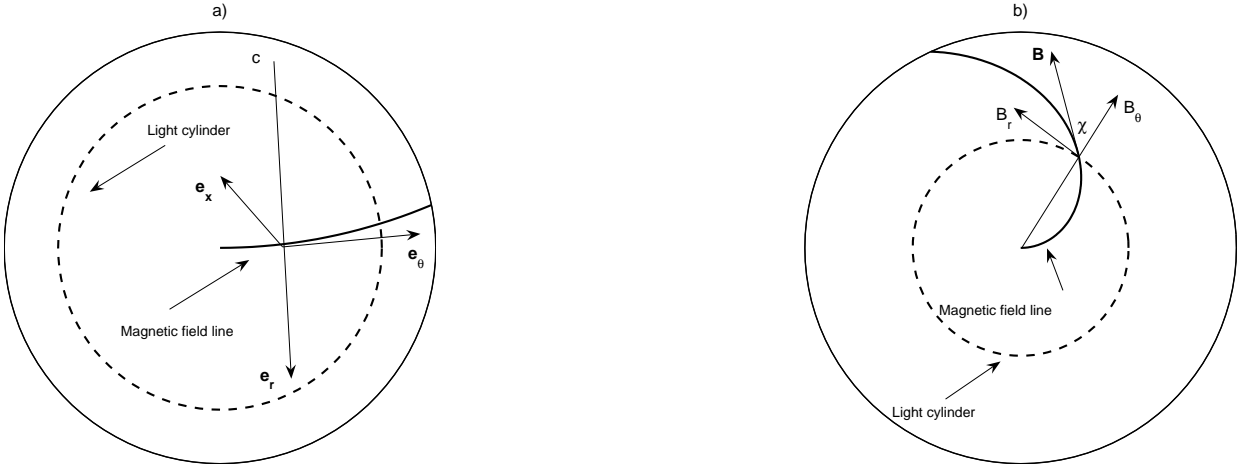


Fig. 4.— *a)* The geometry in which the set of main Eqs. (9-11) is considered ;  $(\mathbf{e}_\theta, \mathbf{e}_r, \mathbf{e}_x)$  denotes orthonormal basis of unit vectors;  $\mathbf{e}_x$  is directed perpendicularly to the plane of the figure; and  $C$  is the center of the curvature. *b)* The geometry for deriving Eq. (32); the curved line denotes the twisted magnetic field,  $\mathbf{B}$ , generated due to the raising of magnetic perturbation,  $\mathbf{B}_r$ .



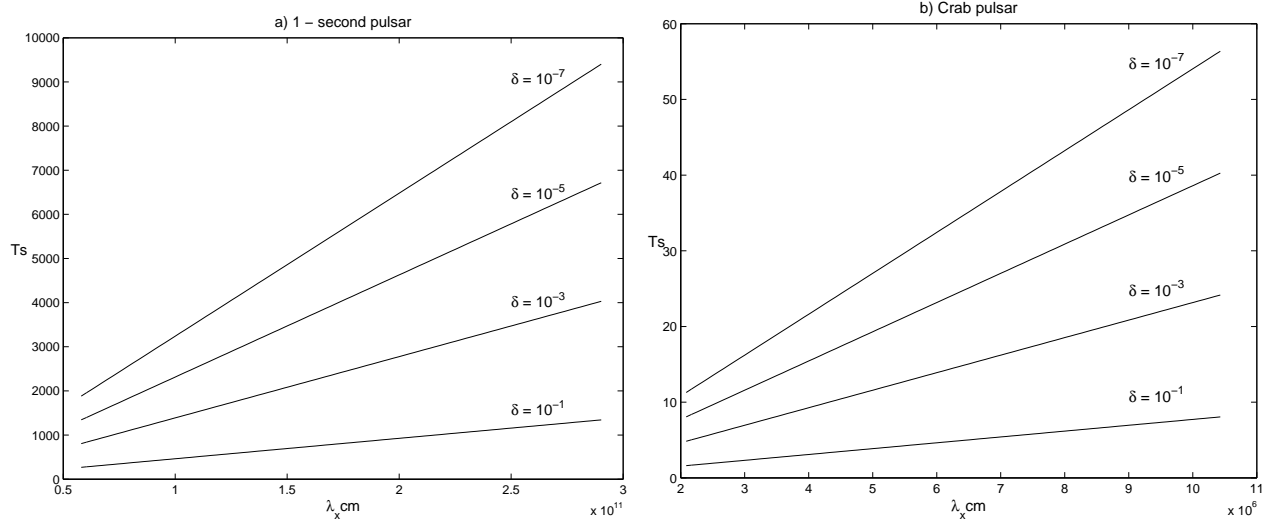


Fig. 5.— Here we show the behaviour of the time scale of sweepback of the magnetic field lines versus the wave length,  $\lambda \approx \lambda_x$ , for the *1-second* pulsar [see (a)] and the Crab pulsar  $P \approx 0.033s$  [see (b)] respectively. The set of parameters is:  $\delta = \{10^{-1}; 10^{-3}; 10^{-5}; 10^{-7}\}$ ,  $\gamma_b \sim 10^6$ ,  $\lambda_x \approx \lambda \gamma_b \sim 10^6$ , and  $\lambda_\theta = 1000R_c$ .